Inorganic Chemistry

Article

pubs.acs.org/IC

Tuning the Coordination Geometries and Magnetic Dynamics of $[Ln(hfac)_4]^-$ through Alkali Metal Counterions

Dai Zeng, Min Ren, Song-Song Bao, and Li-Min Zheng*

State Key Laboratory of Coordination Chemistry, School of Chemistry and Chemical Engineering, Nanjing University, Nanjing 210093, China

Supporting Information

ABSTRACT: Four lanthanide compounds with formulas $[Cs\{Dy(hfac)_4\}]$ (**1**), $[Cs\{Er(hfac)_4\}]$ (**2**), $[K\{Dy(hfac)_4\}]$ (**3**), and $[K\{Er(hfac)_4\}]$ (**4**) (hfac = hexafluoroacetylacetone) are reported. Compounds **1** and **2** crystallize in the orthorhombic *Pbcn* space group, while **3** and **4** are in the triclinic $P\bar{1}$ space group. All display chain structures in which the mononuclear $[Ln(hfac)_4]^-$ anions are linked by alkali metal ions. However, the coordination geometries around the Ln atoms are quite different depending on the cation. They adopt a distorted dodecahedron with pseudo-D_{2d} symmetry in the cesium compounds **1** and **2**, while a distorted square-antiprism with pseudo-D_{4d} symmetry is adopted in the potassium compounds **3** and **4**. The latter compounds show distinct field-induced slow magnetization relaxation. The energy barriers are 23.95 and 20.21 K for compounds **3** and **4**, respectively.

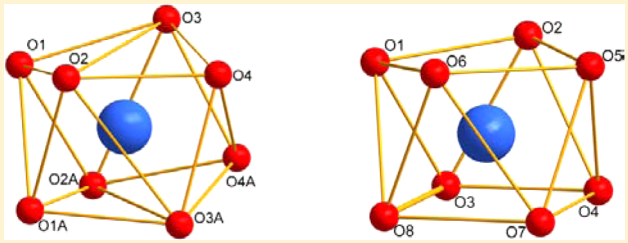

INTRODUCTION

Single-molecule magnets have received great attention due to their potential applications in information storage,[1] molecular spintronics,[2] and quantum computing.[3] In comparison to 3d transition metal ions, lanthanide ions possess significant magnetic anisotropy arising from the large unquenched orbital angular momentum. Since the discovery of $[Pc_2Ln]^-$ as the first single ion magnet by Ishikawa et al. in 2003,[4] a large number of mononuclear lanthanide-based complexes that function as SMMs have been reported, including those containing phthalocyanine,[5] polyoxometalate,[6,7] β-diketone,[8−12] macrocyclic Schiff base,[13,14] or aromatic ligands.[15] In these cases, the magnetic anisotropy required for observing slow magnetic relaxation arises from the splitting of the $2J + 1$ degenerate ground state of the lanthanide ions when it is submitted to a certain ligand field (LF). The splitting generates new ground-multiplet sublevels. This creates an energy gap between the lowest and the second-lowest substates for the spin reversal. Apparently, the ligand field and the coordination geometry pose strong influences on the local anisotropy of the lanthanide ions and, further, on the magnetic dynamics. However, the control of the coordination geometry around the lanthanide ions and the understanding of the relaxation mechanism remain a great challenge.[16] Most work has concentrated on shaping the geometries by using different organic ligands.[16,17]

The β-diketone complexes are one of the representative mononuclear lanthanide compounds for investigating single molecule magnetism. β-Diketone ligands contain stable bidentate chelating sites and can provide suitable ligand fields to study the magnetic anisotropy. A typical example is neutral compound $[Ln(acac)_3(H_2O)_2]$ (acac = acetylacetonate),[8] where the Ln^{3+} ion is surrounded by eight oxygen atoms with a local symmetry of nearly D_{4d}. Magnetic studies on the Dy, Ho, Er analogues reveal that the Dy compound behaves as an SMM with the anisotropy barrier of 66.1 K.[8] The SMM behavior is also found in neutral compounds $[Dy(phen)(acac)_3]$ (phen = *o*-phenanthroline), $[Dy(dpq)(acac)_3]$ (dpq = dipyrido-[3,2-*d*:2′,3′-*f*]-quinoxaline), and $[Dy(dppz)(acac)_3]$ (dppz = dipyrido-[3,2-*a*:2′,3′-*c*]-phenazine), where the phen and its derivatives replace H_2O molecules.[10,11] It is rather interesting to find that the anisotropy energy barriers (63.84, 136, 187 K, respectively) increase with the expansion of the aromatic ring of the phen derivative. The coligand induced tiny distortion of the lanthanide coordination geometry, and its impact on the magnetic dynamics is also demonstrated in the cases of $[Dy(bpy)(TTA)_3]$ and $[Dy(phen)(TTA)_3]$ (TTA = thenoyltrifluoroacetonate).[12]

Another typical compound of β-diketone is formulated as (cation)$[Ln(\beta\text{-diketone})_4]$ which contains an anionic monomer of $[Ln(\beta\text{-diketone})_4]^-$. The lanthanide ion is surrounded by four β-diketone forming a LnO_8 environment. The geometry of the LnO_8 could be affected by the particular cation employed. Nevertheless, detailed magnetic studies on such compounds are still rare. As far as we are aware, only one example, $[Cs\{Dy(Ph2acac)_4\}]_n$ (Ph2acac = dibenzoylmethanide),[18] was reported to show slow magnetization relaxation.

In this Article, we present the syntheses and structural characterization of four lanthanide-β-diketone compounds, namely, $[Cs\{Dy(hfac)_4\}]$ (**1**), $[Cs\{Er(hfac)_4\}]$ (**2**), $[K\{Dy(hfac)_4\}]$ (**3**), and $[K\{Er(hfac)_4\}]$ (**4**) (hfac = hexafluoroacetylacetone). The LnO_8 geometries are found to be dependent

Received: August 17, 2013
Published: January 6, 2014

   dx.doi.org/10.1021/ic402111v | *Inorg. Chem.* 2014, 53, 795−801

on the particular alkali metal ions, which influence the magnetic dynamics of these compounds significantly. It is worth mentioning that structures of [Cs{Ln(hfac)$_4$}] (Ln = Sm,[19] Eu,[20] Nd,[19] Tb,[19] Er,[21] Tm[19]) were reported in the literature, but their magnetic behaviors were unexplored.

EXPERIMENTAL SECTION

Materials and Measurements. All reagents and solvents were purchased from commercial sources and used without further purification. Elemental analyses for C, N, and H were determined with a Perkin-Elmer 240C elemental analyzer. Infrared spectra were recorded on a VECTOR 22 spectrometer with KBr pellets in the range 400−4000 cm^{-1}. Powder X-ray diffraction (PXRD) data were recorded on a Bruker D8 ADVANCE X-ray powder diffractometer (Cu Kα) over the 2θ range 5−50° at room temperature. The magnetization data were recorded on a Quantum Design MPMS-XL7 SQUID magnetometer and a vibrating sample magnetometer (VSM) of Quantum Design MPMS SQUID VSM system. The diamagnetic contribution of the sample itself was estimated from Pascal's constant.[22]

Synthesis of 1−4. Compounds **1**−**4** were synthesized similarly. A typical procedure is described for **1**. A methanol solution (5 mL) of Hhfac (0.4161 g, 2 mmol) and CsOH·H$_2$O (0.3358 g, 2 mmol) was added to a hot solution of Dy(CF$_3$SO$_3$)$_3$ (0.3049 g, 0.5 mmol) in 5 mL of methanol. The mixture was heated to reflux for 3 h under stirring. After cooling to room temperature, the resulting solution was filtered and left to stand at room temperature with slow evaporation. Light yellow rod-like crystals suitable for single crystal X-ray analysis were obtained after 2−3 weeks. Yield: 55%. Elemental analysis calcd (%) for $C_{20}H_4F_{24}O_8DyCs$: C 21.36, H 0.36. Found: C 21.21, H 0.41. IR (KBr, cm^{-1}): 3417(br), 1651(s), 1617(w), 1565(s), 1539(s), 1502(s), 1350(w), 1257(s), 1211(s), 1152(s), 1099(m), 1037(w), 809(s), 770(w), 743(w), 663(s), 588(s), 528(w), 468(w).

For **2**: yield 39%. Elemental analysis calcd (%) for $C_{20}H_4F_{24}O_8ErCs$: C 21.27, H 0.35. Found: C 21.29, H 0.43. IR (KBr, cm^{-1}): 3415(br), 1653(s), 1615(w), 1565(m), 1539(m), 1504(m), 1481(w), 1351(w), 1268(s), 1230(s), 1156(s), 1096(w), 1029(s), 806(w), 761(w), 746(w), 642(s), 575(w), 515(w).

For **3**: yield 49%. Elemental analysis calcd (%) for $C_{20}H_4F_{24}O_8DyK$: C 23.31, H 0.39. Found: C 23.21, H 0.35. IR (KBr, cm^{-1}): 3441(br), 1647(s), 1610(w), 1565(s), 1535(s), 1506(s), 1471(w), 1349(w), 1260(s), 1223(s), 1156(s), 1096(m), 1036(w), 806(s), 770(w), 747(w), 664(s), 590(m), 523(w), 463(w).

For **4**: yield 26%. Elemental analysis calcd (%) for $C_{20}H_4F_{24}O_8ErK$: C 23.20, H 0.39. Found: C 23.02, H 0.37. IR (KBr, cm^{-1}): 3441(br), 1650(s), 1612(w), 1564(s), 1538(s), 1505(s), 1473(w), 1393(w), 1350(w), 1258(s), 1225(s), 1156(s), 1102(m), 1042(w), 806(s), 770(w), 745(w), 664(s), 590(m), 529(w), 468(w).

X-ray Crystallographic Analyses. Single crystals of dimensions 0.45 × 0.25 × 0.25 mm^3 for **1**, 0.40 × 0.25 × 0.25 mm^3 for **3**, and 0.40× 0.22 × 0.22 mm^3 for **4** were mounted on a glass rod. The crystal data were collected on a Bruker SMART APEX DUO diffractometer using monochromated Mo Kα radiation (λ = 0.710 73 Å) at 123 K (for **1**), and Bruker SMART APEX II diffractometer using monochromated Mo Kα radiation (λ = 0.710 73 Å) at 153 K (for **3** and **4**). The numbers of observed and unique reflections are 22 745 and 3066 (R_{int} = 0.041) for **1**, 8742 and 5908 for **3** (R_{int} = 0.007), and 9460 and 6107 (R_{int} = 0.035) for **4**. The structures were solved by direct methods and refined on F^2 by full matrix least-squares using *SHELXTL*.[23] All non-hydrogen atoms were refined anisotropically. All hydrogen atoms were either put in calculated positions or found from the difference Fourier maps and refined isotropically. The F atoms in compounds **1** and **4** are disordered over two sites with a different occupation factor. Details of the crystal data and refinements are summarized in Table 1. Selected bond lengths and angles are given in Supporting Information Tables S1−S3. For comparison, the structure of **2** was also measured at 123 K. The crystal data and structural parameters of **2** are provided in Supporting Information Tables S4 and S5.

Table 1. Crystallographic Data for 1, 3, 4

	1	3	4
empirical formula	$C_{20}H_4CsDyF_{24}O_8$	$C_{20}H_4KDyF_{24}O_8$	$C_{20}H_4KErF_{24}O_8$
fw	1123.64	1029.83	1034.59
cryst syst, space group	orthorhombic, *Pbcn*	triclinic, $P\bar{1}$	triclinic, $P\bar{1}$
a (Å)	8.5259(8)	11.7644(17)	11.799(2)
b (Å)	21.272(2)	12.1610(19)	12.305(3)
c (Å)	17.2044(16)	13.3468(12)	13.428(3)
α (deg)	90	73.298(2)	72.398(3)
β (deg)	90	65.509(3)	65.675(3)
γ (deg)	90	63.667(2)	63.447(3)
V (Å^3), Z	3120.2(5), 4	1544.8(4), 2	1572.3(6), 2
D_c (g cm^{-3})	2.392	2.214	2.185
μ (mm^{-1})	3.732	2.742	2.987
F (000)	2100	978	982
R1[a], wR2[b] [$I > 2\sigma(I)$]	0.0333, 0.1151	0.0539, 0.1356	0.0595, 0.1550
R1[a], wR2[b] (all data)	0.0365, 0.1194	0.0567, 0.1369	0.0680, 0.1623
GOF	1.083	1.191	1.030
($\Delta\rho$)max, ($\Delta\rho$)min (e Å^{-3})	1.33, −0.88	1.17, −0.86	5.16, −1.93
CCDC number	954107	954106	954108

[a]R1 = $\Sigma||F_o| - |F_c||/\Sigma|F_o|$. [b]wR2 = $[\Sigma w(F_o^2 - F_c^2)^2/\Sigma w(F_o^2)^2]^{1/2}$.

RESULTS AND DISCUSSION

Crystal Structures of 1 and 2. Single-crystal structural analyses reveal that compound **1** crystallizes in the orthorhombic system with a *Pbcn* space group, isostructural to **2**.[19] The structure of **1** consists of a [Dy(hfac)$_4$]$^-$ anion, charge-balanced by a cesium cation (Figure 1a). The Dy^{3+} center is chelated by eight oxygen atoms (O1, O2, O3, O4 and O1A, O2A, O3A, O4A) from four hfac$^-$ ligands. The distances of Dy−O bonds vary from 2.323(3) Å to 2.380(3) Å (Supporting Information Table S1), which falls within normal range.[8,9c,e,11] The O−Dy−O angles vary from 72.05(9)° to 150.53(10)°. From continuous shape measure (CSM) analysis,[24] the value obtained relative to the dodecahedron is 0.177 96, which is smaller than 1.837 31 relative to the square antiprism (Table 2). Thus, we can determine the geometry of the octacoordinated dysprosium ion as a distorted dodecahedron with D_{2d} symmetry. The cesium atom is coordinated by six oxygen and six fluorine atoms from bridging hfac$^-$ ligands. The Cs−O and Cs−F distances are 3.189(3)−3.424(3) Å and 3.120(4)−3.351(6) Å, respectively.

There are two crystallographically distinguished hfac$^-$ ligands. One adopts a μ-κ^2-κ^2 coordination mode with the two oxygen atoms of hfac$^-$ bridging both the dysprosium and the cesium atoms (Scheme 1a). The other adopts a μ-κ^2-κ^1 coordination mode with only one oxygen atom involved in bridging Dy and Cs ions (Scheme 1b). As a result, the dysprosium and cesium atoms are connected alternately by the hfac$^-$ ligands, leading to an infinite chain running along the *a*-axis (Figure 2a). The coordination chain is aligned in a zigzag fashion which is reflected by the angle of Cs−Dy−Cs 154.438(2)°. The Dy···Dy distance within the chain is 8.5259(8) Å. The van der Waals interactions are dominant between the chains. The nearest interchain Dy···Dy distance is 11.6595(9) Å.

dx.doi.org/10.1021/ic402111v | Inorg. Chem. 2014, 53, 795−801

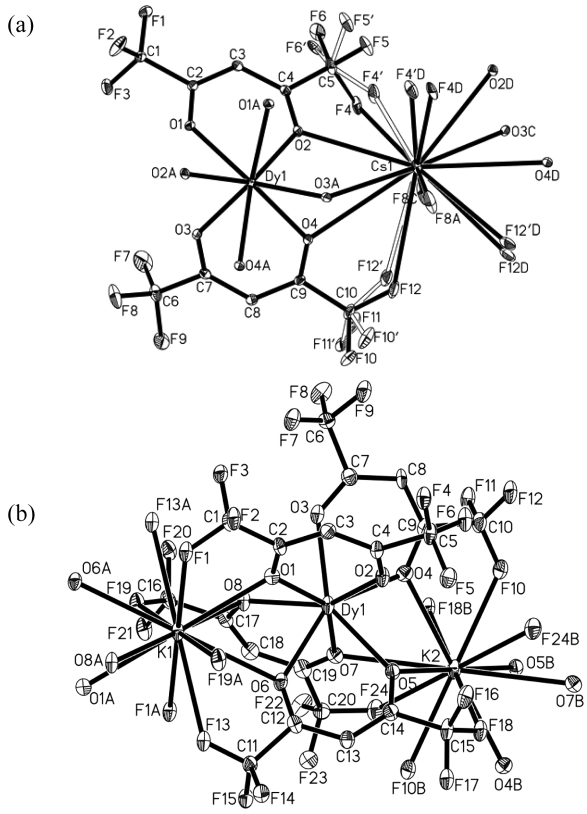

Figure 1. Building unit of compounds **1** (a) and **3** (b) with atomic labeling scheme (30% probability). All H atoms are omitted for clarity.

Table 2. Lanthanide Geometry Analysis by SHAPE Software

CSM	1	2	3	4
antisquare prism (D_{4d})	1.837 31	1.999 89	0.400 73	0.346 39
dodecahedron (D_{2d})	0.177 96	0.129 44	1.586 69	1.526 84

Scheme 1. Coordination Modes of hfac$^-$ (Ln = Dy, Er; A = K, Cs)

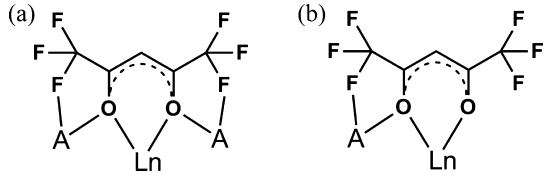

For compound **2**, the $[Er(hfac)_4]^-$ instead of $[Dy(hfac)_4]^-$ is involved. The Er^{3+} center is again octacoordinated with a distorted dodecahedron. The Er−O bond lengths and O−Er−O angles are 2.314(5)−2.358(5) Å and 71.81(18)−150.44(19)°, respectively.

Crystal Structures of 3 and 4. Compounds **3** and **4** are isostructural and crystallize in the triclinic $P\bar{1}$ space group; thus, only the structure of **3** is described in detail. The asymmetric unit of **3** contains one Dy, two K (each with 50% occupancy), and four hfac$^-$ ligands (Figure 1). The Dy^{3+} ion is eight-coordinated, surrounded by all the oxygen atoms from four hfac$^-$ ligands. The Dy−O bond lengths and O−Dy−O angles are 2.299(5)−2.384(4) Å and 70.94(16)−147.99(15)°, respectively (Supporting Information Table S2). The coordination geometry around the Dy^{3+} ion is approximately square-antiprism with D_{4d} symmetry, as suggested by SHAPE software analysis (Figure 3b, Table 2).

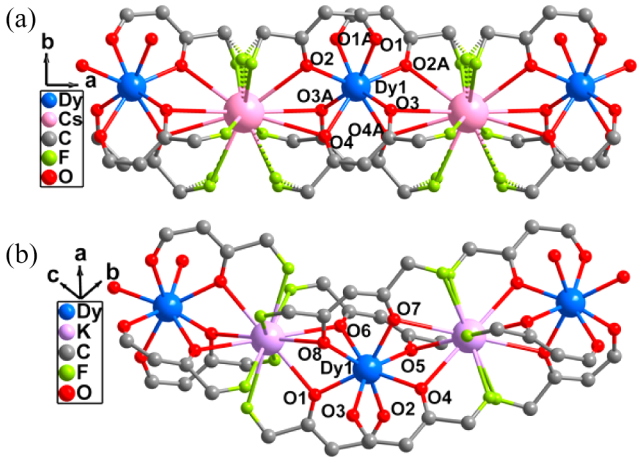

Figure 2. Fragment of one-dimensional chain in structures **1** (a) and **3** (b). All H and F atoms except those involved in the coordination are omitted for clarity.

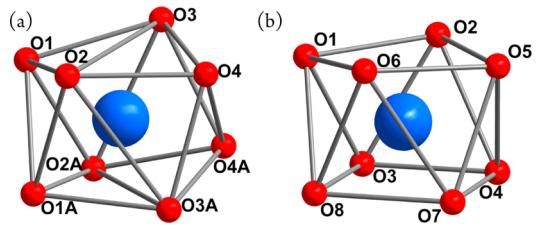

Figure 3. Local coordination geometry of Dy^{3+} ion in **1** (a) and **3** (b).

There are four crystallographically different hfac$^-$ ligands in structure **3**; each chelates the Dy atom through its two oxygen atoms, hence forming a $[Dy(hfac)_4]^-$ anion. The $[Dy(hfac)_4]^-$ anion serves as a metallo-ligand and coordinates to the potassium ion *via* six oxygen and six fluorine atoms [K−O, 2.793(5)−2.998(4) Å; K−F, 2.777(5)−3.035(5) Å]. An infinite chain is thus constructed (Figure 2b). The van der Waals interactions are dominant between the chains. The shortest Dy···Dy distances are 7.9678(7) Å within the chain and 10.1057(9) Å between the chains.

Compound **4** shows an identical chain structure to that of **3** except that the $[Er(hfac)_4]^-$ is involved. In this case, the Er−O bond lengths and O−Er−O bond angles are 2.287(8)−2.377(6) Å and 71.5(3)−147.6(2)°, respectively. The coordination geometry around Er^{3+} is close to a square-antiprism (Table 2).

It is clear that all these four compounds show similar zigzag chain structures with the alkali metal atoms and lanthanide atoms aligning in an alternating fashion. The lanthanide atoms are octacoordinated, consisting of eight oxygen atoms from the hfac$^-$ ligands. The most significant structural difference is that the coordination geometry of the O_8 environment around lanthanide ion. For compounds **1** and **3** which contain the same $[Dy(hfac)_4]^-$ anion, a dodecahedron geometry is found in **1** when Cs^+ ion is used as the charge-balance cation, while a distorted square antiprism is observed in **3** when the cation is K^+. The same phenomenon is also found for compounds **2** and **4** which concern the same $[Er(hfac)_4]^-$ anion. As both Cs^+ and K^+ are coordinated to six oxygen and six fluoride atoms in **1**−**4**,

dx.doi.org/10.1021/ic402111v | Inorg. Chem. 2014, 53, 795−801

the different ionic radii of Cs^+ (1.67 Å for CN = 6) and K^+ (1.38 Å for CN = 6)[25] should be responsible to the different geometries of the Ln^{3+} ions in **1**–**4**. The Cs^+ with larger ionic radii promotes the formation of $\{LnO_8\}$ in pseudo-D_{2d} symmetry, while the K^+ with smaller ionic radii leads to the formation of $\{LnO_8\}$ in pseudo-D_{4d} symmetry.

An ideal square-antiprism (SAP) geometry with D_{4d} symmetry can be recognized by the skew angle $\Phi = 45°$ and the magic angle $\alpha = 54.74°$, as defined in Figure 4. More obtuse

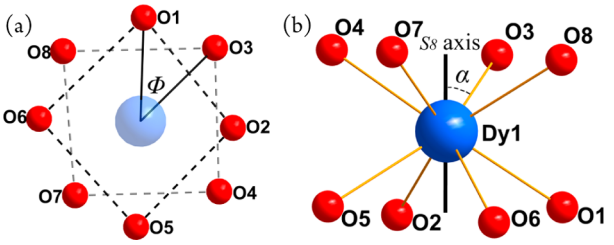

Figure 4. (a) Square-antiprismatic environment with angle Φ between the diagonals of the two squares. (b) Angle α between the S_8 axis and a Dy–O vector.

and acute angles α correspond to compression and elongation, respectively.[17] In the cases of compounds **3** and **4**, the skew angles are 41.31° and 40.46°, respectively, which deviate slightly from the ideal SAP. The α angles are 53.59–61.27° for **3** and 54.56–60.39° for **4** (Figure 4b), indicating that the SAP polyhedra in **3** and **4** are slightly compressed. The presence of pseudo-D_{4d} symmetry in **3** and **4** reminds us of the other acac-based SMMs which exhibit SMM behaviors.[8,9a,b,10–12]

Magnetic Properties of 1 and 3. The direct-current (dc) magnetic susceptibility studies of **1** and **3** were carried out in the temperature range 2–300 K under an applied field of 1 kOe. As shown in Figure 5, the room temperature $\chi_M T$ values

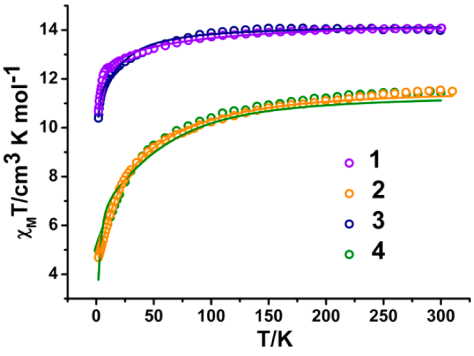

Figure 5. Temperature dependence of $\chi_M T$ products for **1**–**4**.

are 14.08 and 14.00 cm^3 K mol^{-1} for **1** and **3**, respectively, which are in agreement with the expected value of 14.17 cm^3 K mol^{-1} for an isolated Dy^{3+} ($^6H_{15/2}$, $S = 5/2$, $L = 5$, $J = 15/2$, $g = 4/3$). On cooling, $\chi_M T$ values decrease gradually and then rapidly below 50 K, which may be attributed to the progressive depopulation of the excited M_J sublevels.[16b] The magnetic susceptibility data in the high temperature region (>50 K) obey the Curie–Weiss law with the Weiss constant (θ) being −4.00 and −2.03 K for **1** and **3**, respectively (Supporting Information Figures S5 and S7). The magnetization curves of **1** and **3**, measured at 1.8 K, show a rapid increase at low field and then slowly reach the corresponding maximum values of 6.17 and 6.12 $N\beta$ at 70 kOe for **1** and **3**, respectively. These values are lower than the expected saturation value of 10 $N\beta$ for an isolated Dy^{3+}. The nonsuperimposed M versus H/T curves confirm the presence of magnetic anisotropy and/or thermal depopulation of the M_J sublevels in these compounds (Supporting Information Figure S10).[26]

To investigate the magnetization dynamics, the temperature dependent alternating-current (ac) susceptibility data were collected for **1** and **3** at zero dc field with $H_{ac} = 5$ Oe. Neither peaks nor frequency dependence are observed for the in-phase (χ_M') and out-of-phase (χ_M'') signals (Supporting Information Figure S11). It is well-known that the magnetization relaxation of Ln-SMMs could be strongly affected by the quantum tunneling of magnetization (QTM).[27] The QTM effect can be suppressed by applying an external dc field. Thus, the ac measurements were performed at 1.8 K with various applied dc fields in the frequency range 1–1500 Hz on compound **3** (Supporting Information Figure S13a). Attempts to fit these data were unsuccessful due to the broad peaks at high frequency range, so a moderate external field of 2 kOe was selected to measure the ac susceptibility for **1** and **3**.

For compound **1**, both χ_M' and χ_M'' signals are frequency independent, and no peaks appear above 1.8 K (Figure 6, top).

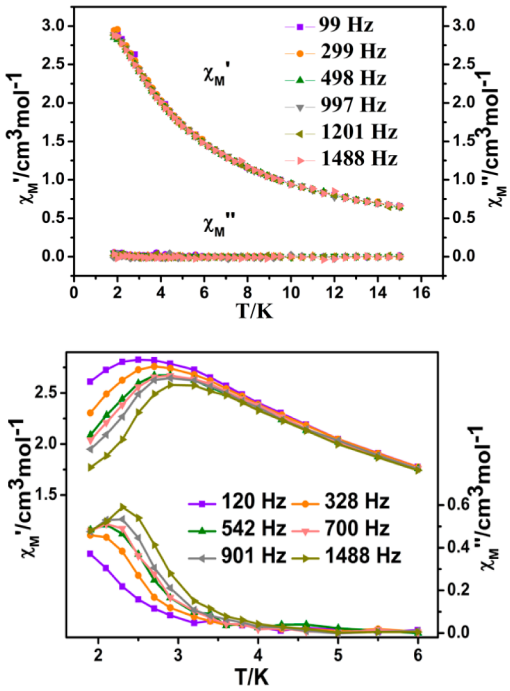

Figure 6. χ_M', χ_M'' versus temperature plots for **1** (top) and **3** (bottom) under 2 kOe field.

While, for compound **3**, frequency dependence of the ac signals appears below *ca.* 4 K, indicating slow relaxation of magnetization (Figure 6, bottom). The peaks in the χ_M'' component can be found at frequencies higher than 328 Hz. The magnetization relaxation times τ are derived from the χ_M'' peaks assuming $\tau = (2\pi\nu)^{-1}$. The relaxation follows a thermally activated mechanism, and data fitting using the Arrhenius law gives an energy barrier of 23.21 K, with the pre-exponential factor τ_0 of 3.91×10^{-9} s (Supporting Information Figure S12).

Frequency dependent ac susceptibilities were also measured for **3** under 2 kOe dc field at various temperatures (1.8–3.0 K). The decline in the χ_M' component concomitant with the appearance of the peaks in the χ_M'' component again indicate

dx.doi.org/10.1021/ic402111v | Inorg. Chem. 2014, 53, 795–801

slow relaxation of magnetization. The magnetization relaxation time τ can be extracted by fitting the Cole−Cole plots using the generalized Debye model for single relaxation process (Figure 7).[28] The distribution coefficient α value is 0.260−0.452 (1.8−3.0 K), indicating that the observed data reasonably fit the theoretical curves (Supporting Information Table S6). The ln τ values increase linearly with the inverse of the temperatures above 2.4 K, and progressively deviate the linearity below 2.4 K due to QTM effects. The slight curvature is likely due to both thermal and QTM mechanisms occurring simultaneously.[29] The Δ/k_B and τ_0 values deduced from the Arrhenius laws using the data of high temperature regime are 23.95 K, and 3.12×10^{-9} s, respectively (Figure 8). The τ_0 value falls in the range for typical SMMs.

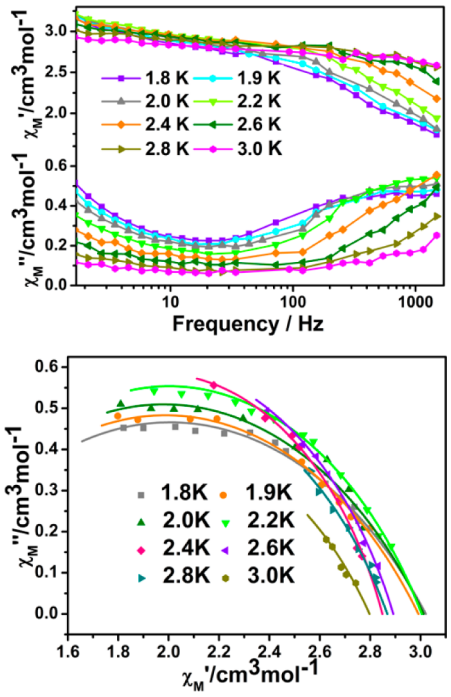

Figure 7. (Top) χ_M', χ_M'' versus frequency plots for **3** under H_{dc} = 2 kOe, H_{ac} = 5 Oe. (Bottom) Cole−Cole plots for **3** obtained using the ac susceptibility data at a 2 kOe dc field.

Magnetic Properties of 2 and 4. The room temperature $\chi_M T$ values of **2** and **4** are 11.50 and 11.45 cm^3 K mol^{-1}, respectively, close to the expected value of 11.48 cm^3 K mol^{-1} for an isolated Er^{3+} ion ($^4I_{15/2}$, $S = 3/2$, $L = 6$, $J = 15/2$, $g = 6/5$). The magnetic susceptibility data in the high temperature region (>50 K) obey the Curie−Weiss law with θ being −18.51 and −15.66 K for **2** and **4**, respectively (Supporting Information Figures S6 and S8). The magnetization reaches 5.15 and 4.67 $N\beta$ at 70 kOe for **2** and **4**, respectively, which are lower values than the theoretical saturation value of 9 $N\beta$ for an isolated Er^{3+}. The unsaturated magnetization at 70 kOe and the nonsuperimposed M versus H/T curves suggest the presence of a large magnetic anisotropy and/or thermal depopulation of the M_J sublevels (Supporting Information Figure S10).

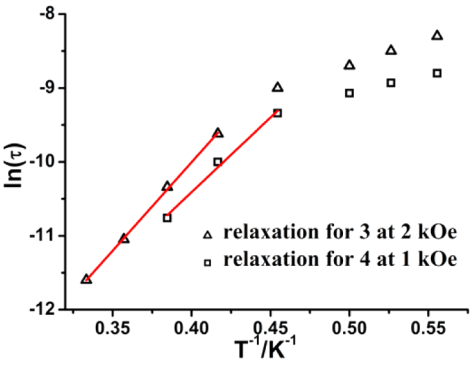

Figure 8. Arrhenius fit of the ln τ vs T^{-1} plots for **3** and **4**.

The ac susceptibility data were collected for **2** and **4** at zero dc field (H_{ac} = 5 Oe). Neither peaks nor frequency dependence for the χ_M' and χ_M'' signals are observed in the temperature dependent plots (Supporting Information Figure S11). To suppress the QTM effect, the ac measurements were recorded in a 1 kOe dc field. This field was chosen as the optimum field because it induces the slowest relaxation (Supporting Information Figure S13b). For compound **2**, only tails of χ_M'' signals are observed below *ca.* 3 K, possibly due to the presence of a slow relaxation of the magnetization (Figure 9, top). For compound **4**, the ac signals become frequency-dependent below *ca.* 4 K (Figure 9, bottom). However, the absence of the distinct peaks of the χ_M'' signals above 1.8 K makes it impossible to estimate the energy barrier by fitting the Arrhenius expression.

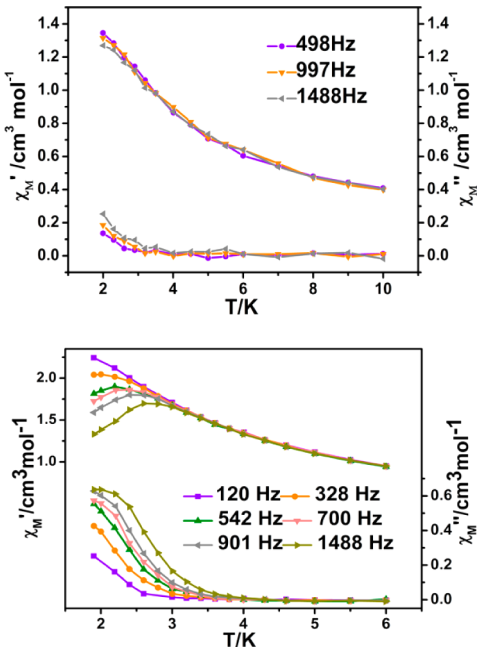

Figure 9. χ_M', χ_M'' versus temperature plots for **2** (top) and **4** (bottom) under 1 kOe field.

Variable frequency dependent ac susceptibilities were also measured in the temperature range 1.8−3.0 K, as shown in Figure 10. Slow magnetization relaxation is clearly observed. The data of Cole−Cole plots can be fitted by the generalized Debye model for single relaxation process. The fitting results are given in Supporting Information Table S7. The distribution coefficient α value is 0.127−0.239 (1.8−2.6 K), indicating a narrow width of the distribution relaxation process. From these data, the relaxation time τ can be deduced. The effective energy barrier is obtained according to Arrhenius law from the high

dx.doi.org/10.1021/ic402111v | Inorg. Chem. 2014, 53, 795−801

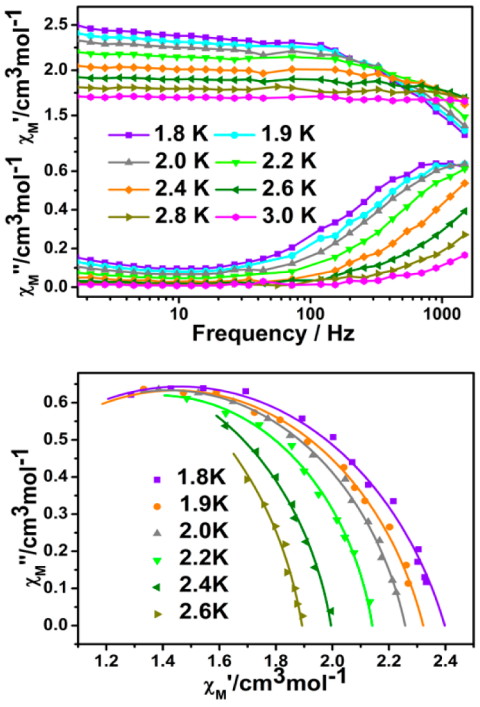

Figure 10. (Top) χ_M', χ_M'' versus frequency plots for **4** under H_{dc} = 1 kOe, H_{ac} = 5 Oe. (Bottom) Cole–Cole plots for **4** obtained using the ac susceptibility data at a 1 kOe dc field.

temperature data as Δ/k_B = 20.21 K (τ_0 = 1.02 × 10^{-8} s) (Figure 8).

Clearly, slow magnetization relaxation characteristic of SMM behavior can be observed for compounds [K{Dy(hfac)$_4$}] (**3**) and [K{Er(hfac)$_4$}] (**4**) below *ca.* 4 K, while not obvious for [Cs{Dy(hfac)$_4$}] (**1**) and [Cs{Er(hfac)$_4$}] (**2**) above 1.8 K. Such a difference can be attributed to the different local environments of Ln^{3+} in **1**–**4**. As described above, the coordination geometry is a distorted dodecahedron with pseudo-D_{2d} symmetry in **1** and **2**, while there is a distorted square-antiprism with pseudo-D_{4d} symmetry in **3** and **4**. In the latter cases, the magnetic anisotropy is significantly enhanced compared with those in **1** and **2**. The results demonstrate that the ligand field of lanthanide ions, and, hence, the magnetic dynamics of the (cation)[Ln(β-diketone)$_4$] systems, can be modulated by using different alkali metal cations.

It would be of interest to compare the magnetic behaviors of **3** and **4** with the related β-diketone-based complexes. In the compounds [Dy(acac)$_3$(H$_2$O)$_2$],[8] [Dy(phen)(acac)$_3$],[10] [Dy(bpy)(tta)$_3$],[12] [Dy(phen)(tta)$_3$],[12] [Dy(dpq)(acac)$_3$],[11] and [Dy(dppz)(acac)$_3$],[11] the central Dy^{3+} ion also shows an approximate D_{4d} symmetry. All exhibit slow relaxation of magnetization under zero dc field with the energy barriers of 63.8–187 K. Slow relaxation of magnetization under zero dc field was also observed in compound [Cs{Dy(Ph$_2$acac)$_4$}]$_n$.[18] In contrast, only field-induced SMM behaviors are found in compounds **3** and **4** with a relatively small energy barriers (23.95 K for **3**, 20.21 K for **4**). The difference could mainly arise from the different ligand field strength around the Dy^{3+} ion induced by the $hfac^-$ ligands as well as the counter cations.

To better understand the different magnetic behavior caused by different alkali metal ions, the electronic fine structures of compounds **1**–**4** are investigated by fitting the $\chi_M T$ versus T curves using Condon package.[30] The Hamiltonian includes zero level energy ($\mathbf{H}_0$), interelectronic repulsion ($\mathbf{H}_{ee}$), spin–orbit effect ($\mathbf{H}_{SO}$), crystal field effect ($\mathbf{H}_{CF}$), and Zeeman effect ($\mathbf{H}_M$). The definition of crystal parameters used here are that of Wybourne.[31] The crystal field operator of f electrons reads, omitting B_0^0, is

$$\hat{H}_{CF} = \sum_{k=2,4}^{6} [B_0^k \hat{C}_0^K(i) + \sum_{q=2,3,4,6}^{k} (B_q^k [\hat{C}_{-q}^k(i) + (-1)^q \hat{C}_q^k(i)])] \quad (1)$$

For compounds **1** and **2** with an approximate dodecahedron D_{2d} symmetry, the Wybourne notation B_0^2, B_0^4, B_4^4, B_0^6, B_4^6 have the nonzero values, while only B_0^2, B_0^4, B_0^6 are effective for **3** and **4** with an approximate square antiprism D_{4d} symmetry. The good fit results can be obtained from a set of crystal field parameters (Figure 5, Table 3). With this set of parameters, it is possible to reproduce the field dependence of the magnetization at 1.8 K, although deviation is visible at higher external fields (Supporting Information Figure S9).

Table 3. Crystal Field Parameters Determined for 1–4

	1	2	3	4
B_0^2	659.8	−421.9	739.9	2177.3
B_0^4	−971.0	−95.6	−1190.2	−461.7
B_4^4	−470.0	3.1		
B_0^6	−442.6	24.6	847.7	1146.8
B_4^6	727.3	716.3		
SQX[a]	4.8 × 10^{-3}	8.2 × 10^{-3}	6.1 × 10^{-3}	12.1 × 10^{-3}

[a] SQX = $(\Sigma_{i=1}^{n}([\chi_{obs}(i) - \chi_{calc}(i)]/\chi_{obs}(i))^2)^{1/2}$.

Supporting Information Tables S8–S10 give the M_J sublevels of the four compounds determined by the crystal field parameters. As shown in Supporting Information Table S8, both **1** and **3** show the ground state of $M_J = \pm 11/2$ doublet mixed with a very small amount of $M_J = \pm 1/2$ doublet, which is not common for the dysprosium based SMMs with uniaxial anisotropy. The first excited state is $M_J = \pm 15/2$ in both cases. The second excited state is a mixture of $M_J = \pm 13/2$ and $M_J = \pm 3/2$ for compound **1** and $M_J = \pm 9/2$ and $M_J = \pm 1/2$ for compound **3**, respectively. The smaller $|M_J|$ value of the ground state (11/2) than that of the first excited state (15/2) suggests that the Dy^{3+} complexes **1** and **3** do not show typical Ising type uniaxial anisotropy. This result may explain the absence of slow magnetization relaxation under zero dc field in both cases.

If we compare the energy gap between the ground state and the first excited state in the two cases, we find that the gap for compound **1** (8.39 cm^{-1} or 12.07 K) is much larger than that for compound **3** (0.16 cm^{-1} or 0.23 K). The large energy gap in **1** cannot be overcome simply by applying an external field of 2 kOe, considering that the magnetic energy for H = 2 kOe is *ca.* 0.27 K. Hence no slow relaxation of magnetization is observed in **1** under 2 kOe dc field. For **3**, however, the $M_J = \pm 15/2$ doublet which is favorable for SMM behavior in many Dy complexes[16,17] lies in the first excited state with a very small energy gap of 0.23 K, which can be overcome by applying an external field of 2 kOe. Above this external field, the state of $M_J = \pm 15/2$ Kramers doublet becomes the ground state. Thus, the Ising-type SMM behavior is switched on in compound **3**. Compared with the other Ln-based SMMs with approximate D_{4d} symmetry,[6–12] the blocking temperature observed for compound **3** is very low, which could be attributed to the

dx.doi.org/10.1021/ic402111v | *Inorg. Chem.* 2014, 53, 795–801

quantum tunneling of the magnetization due to the mixing of several M_J sublevels in the ground state and the low-lying first excited state.

For the erbium-based compounds **2** and **4**, the electronic fine structures are also estimated. As shown in Supporting Information Tables S9 and S10, both the ground state and the excited states contain a mixture of many M_J sublevels. Obviously, the Er^{3+} complexes **2** and **4** do not show typical Ising type uniaxial anisotropy. Therefore, it is reasonable that slow magnetization relaxation under zero dc field is absent in both cases. The observation of field-induced SMM behavior in **4** cannot be explained at this stage. Further in-depth studies as well as ab initio calculations are required to corroborate this proposal.

CONCLUSIONS

We have synthesized and characterized four β-diketone-based lanthanide compounds $[Cs\{Dy(hfac)_4\}]$ (**1**), $[Cs\{Er(hfac)_4\}]$ (**2**), $[K\{Dy(hfac)_4\}]$ (**3**), and $[K\{Er(hfac)_4\}]$ (**4**), three of which are new. The $\{LnO_8\}$ geometries and hence the magnetic anisotropy in these complexes are significantly influenced by different alkali metal ions. Field-induced SMM behaviors are observed for **3** and **4**, while not obvious for **1** and **2**. This work provides a new route to modulate the magnetic dynamics of Ln-SMMs.

ASSOCIATED CONTENT

Supporting Information

Structural data, IR, PXRD, and additional magnetic data. Crystallographic data in CIF format. This material is available free of charge via the Internet at http://pubs.acs.org.

AUTHOR INFORMATION

Corresponding Author

*E-mail: lmzheng@nju.edu.cn.

Notes

The authors declare no competing financial interest.

ACKNOWLEDGMENTS

This work is supported by the National Basic Research Program of China (2010CB923402, 2013CB922102), the NSF of China (11079021), and the NSF of Jiangsu Province of China (BK20130054).

REFERENCES

(1) Yamanouchi, M.; Chiba, D.; Matsukura, F.; Ohno, H. *Nature* **2004**, *428*, 539−542.
(2) Bogani, L.; Wernsdorfer, W. *Nat. Mater.* **2008**, *7*, 179−186.
(3) Leuenberger, M. N.; Loss, D. *Nature* **2001**, *410*, 789−793.
(4) Ishikawa, N.; Sugita, M.; Ishikawa, T.; Koshihara, S.; Kaizu, Y. *J. Am. Chem. Soc.* **2003**, *125*, 8694−8695.
(5) Ishikawa, N.; Sugita, M.; Ishikawa, T.; Koshihara, S.; Kaizu, Y. *J. Phys. Chem. B* **2004**, *108*, 11265−11271.
(6) AlDamen, M. A.; Clemente-Juan, J. M.; Coronado, E.; Marti-Gastaldo, C.; Gaita-Ariño, A. *J. Am. Chem. Soc.* **2008**, *130*, 8874−8875.
(7) AlDamen, M. A.; Cardona-Serra, S.; Clemente-Juan, J. M.; Coronado, E.; Gaita-Ariño, A.; Marti-Gastaldo, C.; Luis, F.; Montero, O. *Inorg. Chem.* **2009**, *48*, 3467−3479.
(8) Jiang, S.-D.; Wang, B.-W.; Su, G.; Wang, Z.-M.; Gao, S. *Angew. Chem., Int. Ed.* **2010**, *49*, 7448−7451.
(9) (a) Mei, X.-L.; Ma, Y.; Li, L.-C.; Liao, D.-Z. *Dalton Trans.* **2012**, *41*, 505−511. (b) Liu, C.-M.; Zhang, D.-Q.; Zhu, D.-B. *Inorg. Chem.* **2013**, *52*, 8933−8940. (c) Li, D.-P.; Wang, T.-W.; Li, C.-H.; Liu, D.-S.; Li, Y.-Z.; You, X.-Z. *Chem. Commun.* **2010**, *46*, 2929−2931. (d) Bernot, K.; Pointillart, F.; Rosa, P.; Etienne, M.; Sessoli, R.; Gatteschi, D. *Chem. Commun.* **2010**, *46*, 6458−6460. (e) Li, D.-P.; Zhang, X.-P.; Wang, T.-W.; Ma, B.-B.; Li, C.-H.; Li, Y.-Z.; You, X.-Z. *Chem. Commun.* **2011**, *47*, 6867−6869.
(10) Chen, G.-J.; Gao, C.-Y.; Tian, J.-L.; Tang, J.-K.; Gu, W.; Liu, X.; Yan, S.-P.; Liao, D.-Z.; Cheng, P. *Dalton Trans.* **2011**, *40*, 5579−5583.
(11) Chen, G.-J.; Guo, Y.-N.; Tian, J.-L.; Tang, J.-K.; Gu, W.; Liu, X.; Yan, S.-P.; Cheng, P.; Liao, D.-Z. *Chem.—Eur. J.* **2012**, *18*, 2484−2487.
(12) Bi, Y.; Guo, Y.-N.; Zhao, L.; Guo, Y.; Lin, S.-Y.; Jiang, S.-D.; Tang, J.-K.; Wang, B.-W.; Gao, S. *Chem.—Eur. J.* **2011**, *17*, 12476−12481.
(13) Yamashita, A.; Watanabe, A.; Akine, S.; Nabeshima, T.; Nakano, M.; Yamamura, T.; Kajiwara, T. *Angew. Chem., Int. Ed.* **2011**, *50*, 4016−4019.
(14) Feltham, H. L. C.; Lan, Y. H.; Klower, F.; Ungur, L.; Chibotaru, L. F.; Powell, A. K.; Brooker, S. *Chem.—Eur. J.* **2011**, *17*, 4362−4365.
(15) (a) Jiang, S.-D.; Wang, B.-W.; Sun, H.-L.; Wang, Z.-M.; Gao, S. *J. Am. Chem. Soc.* **2011**, *133*, 4730−4733. (b) Jiang, S.-D.; Liu, S.-S.; Zhou, L.-N.; Wang, B.-W.; Wang, Z.-M.; Gao, S. *Inorg. Chem.* **2012**, *51*, 3079−3087.
(16) (a) Sorace, L.; Benelli, C.; Gatteschi, D. *Chem. Soc. Rev.* **2011**, *40*, 3092−3104. (b) Rinehart, J. D.; Long, J. R. *Chem. Sci.* **2011**, *2*, 2078−2085.
(17) (a) Sessoli, R.; Powell, A. K. *Coord. Chem. Rev.* **2009**, *253*, 2328−2341. (b) Wang, B.-W.; Jiang, S.-D.; Wang, X.-T.; Gao, S. *Sci. China, Ser. B: Chem.* **2009**, *52*, 1739−1758.
(18) Thielemann, D. T.; Klinger, M.; Wolf, T. J. A.; Lan, Y.; Wernsdorfer, W.; Busse, M.; Roesky, P. W.; Unterreiner, A.-N.; Powell, A. K.; Junk, P. C.; Deacon, G. B. *Inorg. Chem.* **2011**, *50*, 11990−12000.
(19) Danford, M. D.; Burns, J. H.; Higgins, C. E.; Stokely, J. R.; Baldwin, W. H. *Inorg. Chem.* **1970**, *9*, 1953−1955.
(20) Burns, J. H.; Danford, M. D. *Inorg. Chem.* **1969**, *8*, 1780−1784.
(21) Tan, R. H. C.; Motevalli, M.; Abrahams, I.; Wyatt, P. B.; Gillin, W. P. *J. Phys. Chem. B* **2006**, *110*, 24476−24479.
(22) Kahn, O. *Molecular Magnetism*; VCH Publishers, Inc.: New York, 1993.
(23) Sheldrick, G. M. *SHELXTL-97*; Universität Göttingen: Göttingen, Germany, 1997.
(24) Casanova, D.; Llunell, M.; Alemany, P.; Alvarez, S. *Chem.—Eur. J.* **2005**, *11*, 1479−1494.
(25) Shannon, R. D. *Acta Crystallogr.* **1976**, *A32*, 751−767.
(26) Abbas, G.; Lan, Y.; Kostakis, G. E.; Wernsdorfer, W.; Anson, C. E.; Powell, A. K. *Inorg. Chem.* **2010**, *49*, 8067−8072.
(27) Thomas, L.; Lionti, F.; Ballou, R.; Gatteschi, D.; Sessoli, R.; Barbara, B. *Nature* **1996**, *383*, 145−147.
(28) (a) Cole, K. S.; Cole, R. H. *J. Chem. Phys.* **1941**, *9*, 341−351. (b) Gatteschi, D. Sessoli, R. Villain, J. *Molecular Nanomagnets*; Oxford University Press: Oxford, U.K., 2006.
(29) Langley, S. K.; Chilton, N. F.; Moubaraki, B.; Murray, K. S. *Chem. Commun.* **2013**, *49*, 6965−6967.
(30) (a) Lueken, H. *Magnetochemie*; Teubner: Stuttgart, 1999. (b) Schilder, H.; Lueken, H. *J. Magn. Magn. Mater.* **2004**, *281*, 17−26. (c) Cardona-Serra, S.; Clemente-Juan, J. M.; Coronado, E.; Gaita-Arino, A.; Camon, A.; Evangelisti, M.; Luis, F.; Martinez-Perez, M. J.; Sese, J. *J. Am. Chem. Soc.* **2012**, *134*, 14982−14990. (d) Liu, J.-L.; Yuan, K.; Leng, J.-D.; Ungur, L.; Wernsdorfer, W.; Guo, F.-S.; Chibotaru, L. F.; Tong, M.-L. *Inorg. Chem.* **2012**, *51*, 8538−8544. (e) Pointillart, F.; Le Guennic, B.; Golhen, S.; Cador, O.; Maury, O.; Ouahab, L. *Chem. Commun.* **2013**, *49*, 615−617. (f) Pointillart, F.; Le Guennic, B.; Cauchy, T.; Golhen, S.; Cador, O.; Maury, O.; Ouahab, L. *Inorg. Chem.* **2013**, *52*, 5978−5990.
(31) Wybourne, B. G. *Spectroscopic Properties of Rare Earths*; Wiley: New York, 1965.